*Journal of Statistical Research* *https://doi.org/10.47302/jsr.2021550110*
*2021, Vol. 55, No. 1, pp. 147-158* *ISSN 0256 - 422 X*

# PROBABILISTIC DIFFUSION MAGNETIC RESONANCE IMAGING FIBER TRACKING USING A DIRECTED ACYCLIC GRAPH AUTO-REGRESSIVE MODEL FOR POSITIVE DEFINITE MATRICES

ZHOU LAN

*Center for Outcomes Research and Evaluation*
*Yale University, New Haven CT 06510, USA*

*Email: zhou.lan@yale.edu*

BRIAN J. REICH

*Department of Statistics*
*North Carolina State University, Raleigh NC 27695, USA*

*Email: brian_reich@ncsu.edu*

DIPANKAR BANDYOPADHYAY*

*Department of Biostatistics*
*Virginia Commonwealth University, Richmond VA 23298, USA*

*Email: dbandyop@vcu.edu*

SUMMARY

Diffusion magnetic resonance imaging (MRI) is a neuroimaging technique for probing the anatomical structure of tissues through quantification of the water diffusion process. Using diffusion MRI to reconstruct white matter fiber tracts and assess tissue connectivity, also known as fiber tracking, is arguably the most important applications of diffusion MRI. Although a number of innovative and compelling techniques are available for fiber tracking, only a few provide an elegant evaluation of the statistical (spatial) uncertainties. In this paper, we propose spatial modeling of positive definite diffusion tensor matrices via a directed acyclic graph auto-regressive model and develop an efficient probabilistic fiber tracking algorithm. We illustrate our proposed method via numerical studies and application to a real dataset.

*Keywords and phrases:* Directed Acyclic Graph Auto-Regressive Model; Diffusion MRI; Fiber Tracking; Positive Definite Matrices

*AMS Classification:* 62H10; 62C10; 62H35

* Corresponding author

# 1 Introduction

In neuroscience, the central objective is to understand and quantify the interactions and information transfer between different cortical regions of the human brain (Behrens et al., 2007). Using the water diffusion process as a proxy, the Diffusion magnetic resonance imaging (dMRI), an in vivo noninvasive neuroimaging technique, allows for identifying the anatomical connections between brain tissues. Fiber tracts within the human brain are large axonal bundles with similar directions. Fiber tractography, a 3D technique to visually represent the underlying white matter fiber tracts, is one of the most important uses of dMRI, and the only way to study brain structural connectivity. Mapping white matter fiber tracts is crucial in studies of neuronal networks, brain functionality, and connectome (Sporns et al., 2005). From the clinical perspective, it may help detect white matter abnormality related to many neuro-degenerative disease (such as Alzheimer's disease) and resolve complex neuronal connections in presurgical planning (Chung et al., 2011).

The dMRI constitutes voxel-wise diffusion weighted signal measurements on a 3D spatial grid (Bammer et al., 2009). The diffusion directions can be estimated by the models (e.g., single tensor model) treating diffusion weighted signal measurements as responses collected voxel-wise. Majority of the current tractography methods (e.g., Wong et al., 2016) mapping white matter fiber tracts follows a 3 step process. In Step 1, voxel-wise diffusion directions are estimated using diffusion-weighted signals. In Step 2, the estimated diffusion directions obtained in Step 1 are smoothed over space. Finally, in Step 3, the smoothed diffusion directions are taken as the inputs of a fiber tracking algorithm that determines if some voxels construct a fiber.

Although the battery of available methods enjoy useful applications to mapping white matter fiber tracts, a vast majority considers a deterministic approach, where a single diffusion orientation (Cheng et al., 2006) of each voxel determines the inference of fiber paths across voxels. However, a single diffusion orientation per voxel may not adequately characterize voxels with fibers of various orientations, such as crossing, branching, fanning, or with bottlenecks. Furthermore, deterministic algorithms can follow false tracts, or stop in regions with isotropic tensors (Descoteaux et al., 2008). On the contrary, the probabilistic approach presents a more flexible route by modeling multiple diffusion orientations per voxel, with the tractography based on a probability distribution of the possible diffusion orientations (Morris et al., 2008; Schlaier et al., 2017).

In light of these, we propose a Bayesian hierarchical approach that allows valid statistical inference for fiber tracking with probabilistic justifications. Our central objective is to improve upon available spatial smoothing techniques (Wong et al., 2016) for precise estimation of diffusion directions via borrowing of information from neighboring voxels. We assume the logarithm of the signals follow a normal distribution, where the latent random field of spatially dependent positive definite (p.d.) matrices induces the spatial smoothness via a directed acyclic graph auto-regressive (DAGAR) proposal (Datta et al., 2019). We call this method as *Spatial Diffusion Direction Smoothing and Tracking*, or `SpDiST` (see Section 2). Under a Bayesian paradigm, we implement Markov chain Monte Carlo (MCMC) sampling for model fitting. Since the fiber tracking algorithm can be applied to each MCMC sample, we can infer results in a probabilistic way. For illustration of our methodology, we use both synthetic and real data. The real data application (Section 3) elucidates our proposal as a reasonable and valid means for probabilistic fiber tract inspection, where various

connection patterns could be identified. The numerical study using synthetic data (in Section 4) shows that our proposal is robust to the signal noises, compared to other alternative methods, such as the least squares method, and the Diffusion Direction Smoothing and Tracking, or `DiST` (Wong et al., 2016). Finally, we conclude with a discussion in Section 5.

# 2 Method: `SpDiST`

## 2.1 Spatial tensor model

In this section, we introduce the spatial tensor model based on the DAGAR proposal for p.d. matrices. The dMRI has $m \in \{1, 2, \ldots, M\}$ measurements at voxel $v \in \{1, 2, \ldots, n\}$, denoted as $S_{mv} \in \mathbb{R}^+$. The measurements $S_{mv}$ are used to estimate the diffusion tensor $\boldsymbol{A}_v$ for voxel $v$. $\boldsymbol{A}_v$ is a $3 \times 3$ p.d. matrix, interpreted as covariance matrix of a local Brownian motion, indicating the local tensor direction. The diffusion tensor of the water molecules at voxel v is denoted $A_v$ and must be a positive definite matrix by definition. The goal is to use the measurements $S_{mv}$ to estimate tensor direction information from $\boldsymbol{A}_v$.

The noiseless signal intensity $\bar{S}_{mv}$ can be expressed in terms of $\boldsymbol{A}_v$ (Mori, 2007) as

$$\bar{S}_{mv} = S_{0v} \exp(-b\boldsymbol{g}_m^T \boldsymbol{A}_v \boldsymbol{g}_m).$$

In this expression, $S_{0v}$, $b$, and $\boldsymbol{g}_m$ are non-diffusion weighted intensity, scale parameter, and $3 \times 1$ unit-norm gradient vector, respectively. A detailed explanation of these three quantities can be found in Soares et al. (2013). Given $\boldsymbol{A}_v$, $\bar{S}_{mv}$ can be interpreted as the probability intensity of the Gaussian motion when measuring at direction $\boldsymbol{g}_v$. For statistical modeling, $S_{0v}$, $b$, and $\boldsymbol{g}_m$ can simply be understood as fixed and known values.

The observations $S_{mv}$ are noisy realizations of $\bar{S}_{mv}$. Here, we assume that the noise is a multiplier to $\bar{S}_{mv}$, following a lognormal distribution. The corresponding model is

$$\log S_{mv} = \log S_{0v} - b\boldsymbol{g}_m^T \boldsymbol{A}_v \boldsymbol{g}_m + \epsilon_{mv}, \quad \epsilon_{mv} \overset{\text{iid}}{\sim} \mathcal{N}(0, \sigma^2), \tag{2.1}$$

where $\epsilon_{mv}$ is the noise following a mean-zero normal distribution with the variance $\sigma^2$.

To induce spatial smoothness, an image is treated as a directed graph whose nodes are voxels and whose directed edges are from node $v$ to nodes in $N(v)$. Following Datta et al. (2019), we use the directed acyclic graph (directed, without loops) to construct $N(v)$, leading to a valid joint density function of $[\boldsymbol{A}_1, \boldsymbol{A}_2, \ldots, \boldsymbol{A}_n]$. In particular, we assume that the conditional mean of $\boldsymbol{A}_v$ is the average of its neighboring tensors, denoted as $\mathbb{E}[\boldsymbol{A}_v | \boldsymbol{A}_u, u \in N(v)] = |N(v)|^{-1} \sum_{u \in N(v)} \boldsymbol{A}_u$, where $N(v)$ is a set containing neighboring voxel indices of voxel $v$, and $|N(v)|$ is the set size.

In a directed acyclic graph, we have at least one voxel $v$ whose $N(v)$ is an empty set. When $N(v)$ is an empty set, we assume that $\boldsymbol{A}_v$ follows a Wishart distribution with mean matrix $\boldsymbol{I}$ and degrees of freedom $k$. Otherwise, conditional on $\boldsymbol{A}_u, u \in N(v)$, we assume $\boldsymbol{A}_v$ follows a Wishart distribution with mean matrix $\bar{\boldsymbol{A}}_v = |N(v)|^{-1} \sum_{u \in N(v)} \boldsymbol{A}_u$ and degrees of freedom $k$. The model is

$$\begin{aligned} \boldsymbol{A}_v | \boldsymbol{A}_u, u \in N(v) &\sim \mathcal{W}\left(\bar{\boldsymbol{A}}_v, k\right) && \text{if } N(v) \text{ is not empty,} \\ \boldsymbol{A}_v &\sim \mathcal{W}(\boldsymbol{I}, k) && \text{if } N(v) \text{ is empty.} \end{aligned} \tag{2.2}$$

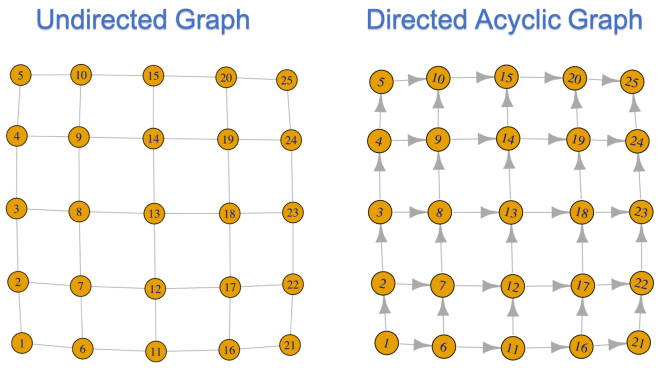


Figure 1: The construction of a directed acyclic graph based on an undirected graph. The left panel is the undirected graph of a $5 \times 5$ image. The right pannel is the corresponding directed acyclic graph after modifying the edges.

To preserve the designed mean realizations in 2.2, we parameterize the Wishart distribution for $\boldsymbol{X} \sim \mathcal{W}(\boldsymbol{V}, k)$ to have $\mathbb{E}\boldsymbol{X} = \boldsymbol{V}$. The probability density function is

$$f(\mathbf{X}) = \frac{|\mathbf{X}|^{(k-p-1)/2}\, e^{-\operatorname{tr}([\mathbf{V}/k]^{-1}\mathbf{X})/2}}{2^{kp/2}\, |\mathbf{V}/k|^{k/2}\, \Gamma_p(\frac{k}{2})},$$

where, $p$ is the matrix dimension and $\Gamma_p(\frac{k}{2})$ is the multivariate gamma function.

Here, we present an approach to construct a directed acyclic graph. For an image, we construct an undirected graph whose voxels are nodes, and the neighboring nodes are connected. We order the voxels by their coordinates. Thus, for a 2D image on a *x*-*y* axis, we first order the voxels according to their coordinates of the *y*-axis, following which, we order the voxels according to their coordinates of the *x*-axis. We modify the undirected edge to a directed edge for each edge of the undirected graph, which is from the node with a smaller rank to a node with a larger rank. The modified graph is a directed acyclic graph whose edges connect neighboring voxels. Figure 1 presents an example describing how a directed acyclic graph for a $5 \times 5$ image is constructed.

For conducting Bayesian inference, we assign priors to the unknown parameters in our model. Because $k$ is a parameter (degrees of freedom) larger than 3, The value of the degrees of freedom $k$ follows a uniform distribution, ranging from 3 to 50, denoted as $k \sim \mathcal{U}(3, 50)$. To provide a conjugate prior, the variance $\sigma^2$ follow a inverse Gamma distribution with the shape parameter 0.01 and the rate parameter 0.01, denoted as $\sigma^{-2} \sim \mathcal{GA}(0.01, 0.01)$.

## 2.2 Markov chain Monte Carlo (MCMC) algorithm

We use MCMC techniques for model fitting. The primary challenge in the MCMC algorithm is to sample from the posterior of $\boldsymbol{A}_v$. Since the prior of $\boldsymbol{A}_v$ is not conjugate, we sample it using single-site Metropolis-Hastings sampling with Wishart distribution $\mathcal{W}(\boldsymbol{A}'_v|\boldsymbol{A}_v, q)$ as the proposal distribution. The algorithm is described below:

**Candidate Generation:** Generate a candidate sample $\boldsymbol{A}'_v$ using $\boldsymbol{A}'_v \sim \mathcal{W}(\boldsymbol{A}'_v|\boldsymbol{A}_v, q)$;

**Acceptance Rate:** Calculate the acceptance rate $r(\boldsymbol{A}'_v, \boldsymbol{A}_v) = \frac{\mathcal{L}(\boldsymbol{A}'_v|\cdot)\,\mathcal{W}(\boldsymbol{A}_v|\boldsymbol{A}'_v,q)}{\mathcal{L}(\boldsymbol{A}_v|\cdot)\,\mathcal{W}(\boldsymbol{A}'_v|\boldsymbol{A}_v,q)}$, where

$$\begin{aligned}\mathcal{L}(\boldsymbol{A}^*_v|.) \propto \prod_{m=1}^{M} \mathcal{N}\big(\log S_{mv}|\log S_{0v} - b\boldsymbol{g}_m^T\boldsymbol{A}^*_v\boldsymbol{g}_m, \sigma^2\big)\times \\ \mathcal{W}(\boldsymbol{A}^*_v|\bar{\boldsymbol{A}}^*_v, q)\prod_{u:v\in N(u)}\mathcal{W}(\boldsymbol{A}_u|\bar{\boldsymbol{A}}^*_u, q),\end{aligned} \tag{2.3}$$

where $\bar{\boldsymbol{A}}^*_u = |N(v)|^{-1}\big(\sum_{u\in N(u)/v}\boldsymbol{A}_u + \boldsymbol{A}^*_v\big)$. $\mathcal{W}(\cdot|\boldsymbol{A},\nu)$ and $\mathcal{N}(\cdot|\mu,\sigma^2)$ are the density functions of Wishart distribution and normal distribution, respectively.

**Decision:** Generate $u \sim \mathcal{U}(0,1)$. If $u < r(\boldsymbol{A}'_v, \boldsymbol{A}_v)$, accept $\boldsymbol{A}'_v$.

The acceptance rate can be tuned via the degrees of freedom $q$, where smaller $q$ leads to a lower acceptance rate. We adjust $q$ to make the acceptance rate around $0.4$. We use Metropolis-Hastings algorithm with log-normal random walk proposals to update the degrees of freedom $q$, and use Gibbs sampling to update $\sigma^2$ based on its posterior

$$[\sigma^{-2}|\cdot] \sim \mathcal{GA}\big(Mn/2 + 0.01, \sum_{m,v}(\log S_{mv} - \log S_{0v} + b\boldsymbol{g}_m^T\boldsymbol{A}_v\boldsymbol{g}_m)^2/2 + 0.01\big).$$

## 2.3 Probabilistic fiber tracking algorithm

We collect the $T$ MCMC samples from the posterior distribution of $\boldsymbol{A}_v$, denoted as $\{\boldsymbol{A}_v^{(t)} : t = 1, 2, \ldots, T\}$. For each sample, we compute the principal eigenvector of $\boldsymbol{A}_v^{(t)}$, denoted as $\boldsymbol{m}_v^{(t)}$. For each posterior draw, we use $\boldsymbol{m}_v^{(t)}$ as inputs of a fiber tracking algorithm. In this paper, we use the Fiber Assignment by Continuous Tracking (FACT) (Mori et al., 1999), following Wong et al. (2016). The algorithm can be stated as

- **Initialization:** Set *seed voxels*;
- **Recursive:** Starting with voxel $u$, we search neighboring voxels, and compute the two angles: $\delta_{uv} = \arccos\left(\frac{\boldsymbol{m}_v^T\boldsymbol{m}_u}{|\boldsymbol{m}_v|\,|\boldsymbol{m}_u|}\right)$, the angle between the two tensor directions ($\boldsymbol{m}_u$ and $\boldsymbol{m}_u$), and $\theta_{uv} = \arccos\left(\frac{\boldsymbol{m}_u^T\boldsymbol{l}_{u,v}}{|\boldsymbol{m}_u|\,|\boldsymbol{l}_{u,v}|}\right)$, the angle between the current tensor ($\boldsymbol{m}_u$) and between-voxel direction ($\boldsymbol{l}_{u,v}$). See Figure 2 for details. We move to the voxels with $\theta < C$ and $\delta < C$. If there are multiple voxels statisfying this condition, we move to all the voxels and treat each voxel as a current voxel for next iteration.;

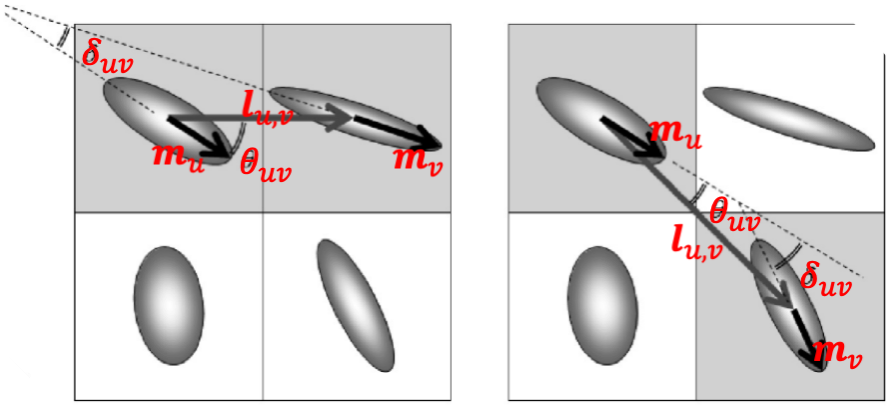


Figure 2: Assessing directional consistency of the two relationships: (a) between the principal eigenvectors (thick black arrows, angle $\delta$) of the 2 voxels, and (b) between the fiber direction and the vector connecting the 2 voxels (thick gray arrow, angle $\theta$). The two voxels are not considered connected (left panel), and exhibit connections (right panel). This figure has been adapted and modified from Chung et al. (2011, Figure 3).

- **Result:** Sequences of voxels constructing *fibers*.

Since we apply the algorithm for each posterior draw, the algorithm returns $T$ possible fiber connections. We summarize $K$ distinct patterns from the outputs. We further calculate the associated probability for pattern $k \in \{1, 2, \ldots, K\}$, defined as $T_k/T$, where $T_k$ is the frequency of the pattern $k$. This procedure is known as *probabilistic fiber tracking* and quantifies the uncertainties of fiber tracking results.

# 3 Real Data Application

In this section, we use a real data example (Dryden et al., 2009, Section 6) to demonstrate our proposed method. In particular, we focus on uncertainty quantification. The real data has $50 \times 20$ voxels, with $M = 15$ measurements. We sample 2000 MCMC samples after discarding 3000 samples as burn-in, and thin the MCMC chain by retaining every 100 iterations of the chain.

Since it is more efficient to visualize tensor directions in a 2D environment and the image is 2D, we focus on the first two dimensions of $\boldsymbol{A}_v$ and compute the corresponding principal eigenvector $\boldsymbol{m}_v$. To quantify the uncertainties of tensor direction estimation in each voxel, we overlay the MCMC samples on a $50 \times 20$ map (Figure 3). We observe that voxels with heterogeneous directions have large uncertainties. Otherwise, the uncertainties are smaller.

Figure 3 only provides voxel-wise uncertainties. However, the MCMC-based `SpDiST` also provides a probabilistic approach to quantifying fiber tracking uncertainties. To have a concise and representative illustration, we focus on the region in the orange box of Figure 3, and apply the FACT algorithm as described in Section 2.3. In light of the suggested values of the threshold $C$

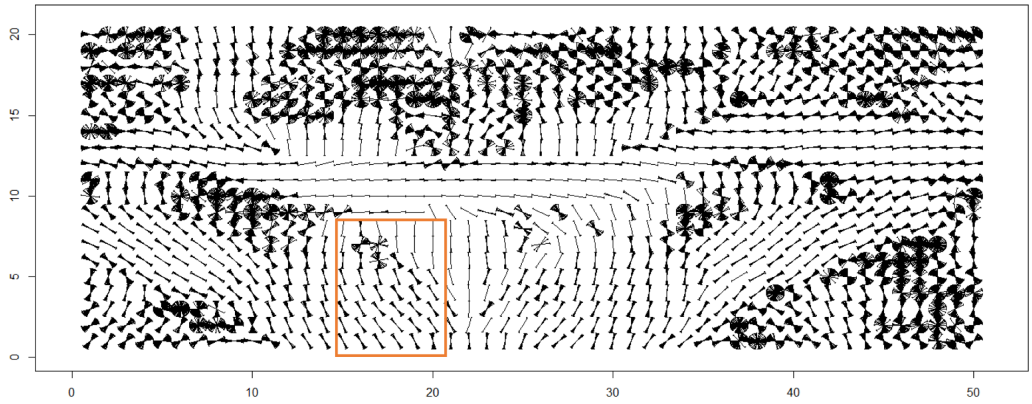


Figure 3: Real Data Application, where, for each voxel, the MCMC samples of $\boldsymbol{m}_v$ are overlaid on its location on a $50 \times 20$ map.

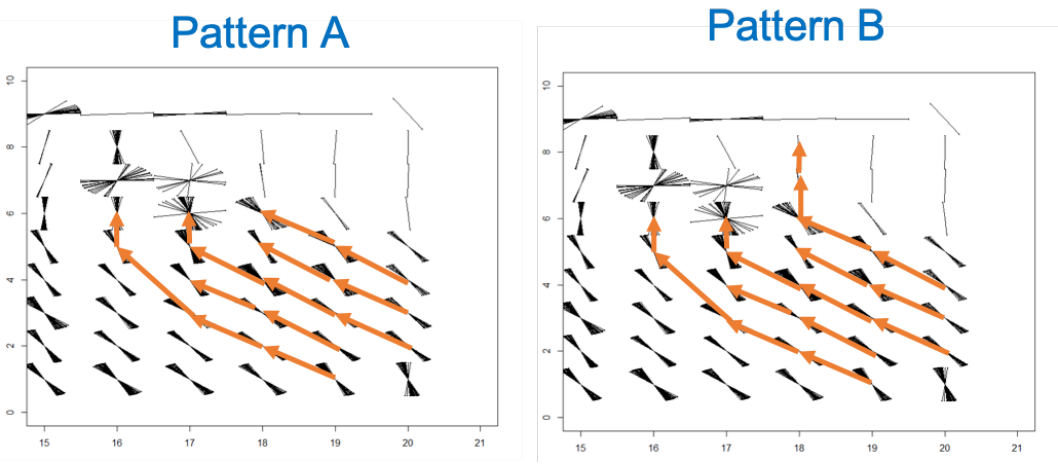


Figure 4: Real Data Application, where the consecutive orange arrows construct a fiber in the region outlined in orange in Figure 3.

(Chung et al., 2011; Wong et al., 2016), we consider $C$ ranging from $18^o$ to $28^o$. We identify two distinct patterns (Pattern A and Pattern B; see left and right panels of Figure 4) for $C \in [18^o, 28^o]$ as dominating the posterior probability of the tract. These two tracts differ only by how far the tract continues vertically in column 18.

Kang and Li (2016, Section 3) show that the FACT algorithm hinges on the tuning parameter $C$. It requires a sensitivity analysis to explore the impact of $C$. Here, we present a sensitivity analysis.

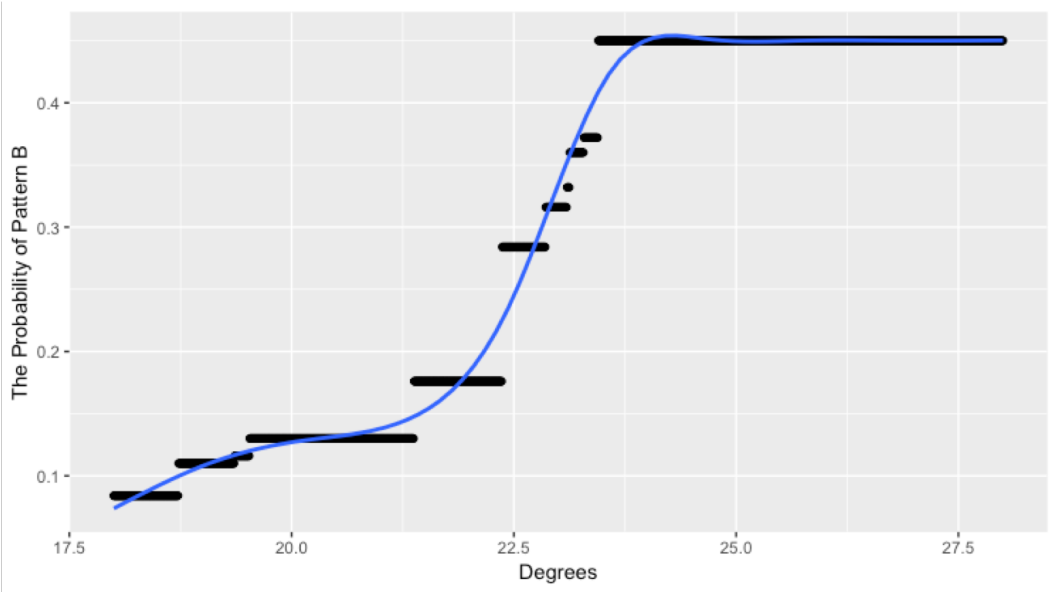


Figure 5: The probability of Pattern B (Figure 4) varies with different threshold $C$. When $C$ is ranging from $24^o$ to $28^o$ the probability is insensitive to $C$.

We apply the FACT algorithm with $C = 18 + 0.01 \times s$ and $s = \{0, 1, 2, \ldots, 1000\}$. Since there are only two distinct patterns, we report Pattern B's probabilities with different thresholds $C$ (Figure 5). We find that the result is sensitive to the choice of $C$, unless it is ranging from $24^o$ to $28^o$.

# 4 Simulation Study

In this section, we use synthetic diffusion-weighted signals as in Wong et al. (2016, S6) and further modify them for our simulation study. In total, we have $8 \times 7 \times 2$ voxels where the three digits represent the dimension of $x$-axis, $y$-axis, and $z$-axis, respectively. The underlying tensors and fibers from the synthetic signals are displayed in Figure 6. A comprehensive description of the data generation can be found in Wong et al. (2016, S6) (i.e., generating model, parameters, true tensor directions, etc.). Here, we give a brief description. The fibers are essentially arcs with the center point at right/left bottom points. Its principal eigenvector $\boldsymbol{m}_v$ is tangent to the arc for voxels composing fibers. The noiseless signal in the example data is given as $\bar{S}_{mv} = S_{0v} \exp[-b(\boldsymbol{g}_m^T \boldsymbol{m}_v)^2]$, a reparameterized model of Model 2.1 (Wong et al., 2016).

To mimic low-quality images with signal noise, we further add noise on the log scale simulated from a mean-zero normal distribution with standard deviation $\tau = 0.1, 0.5$. Thus, the simulated data for each replication ($r = 1, \ldots, 50$) is

$$\log S_{mv}^{(r)} = \log \bar{S}_{mv} + E_{mv}^{(r)}, \quad E_{mv}^{(r)} \sim \mathcal{N}(0, \tau^2), \tag{4.1}$$

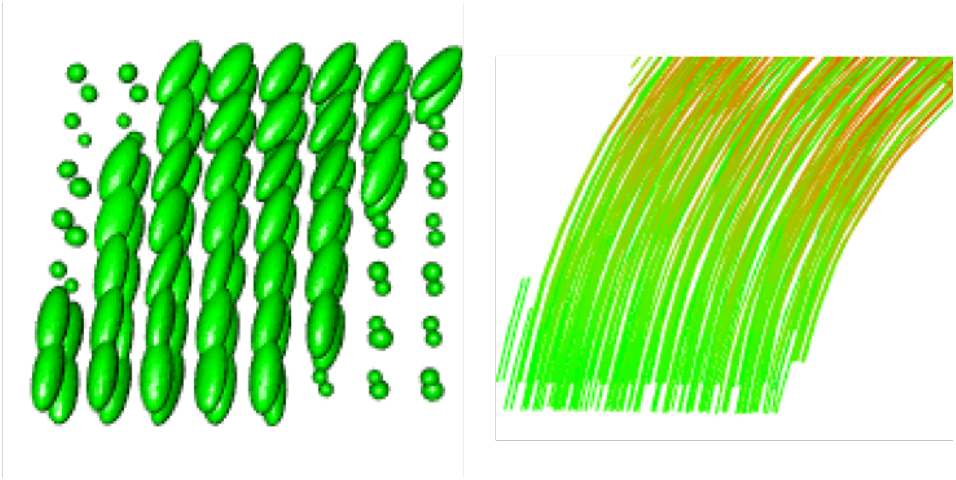

Figure 6: The tensor directions (left panel) and underlying fibers (right panel) from the example data .

where $\log S_{mv}^{(r)}$ is the simulated signals for each replication $(r)$, $\log S_{mv}$ is the logarithm signal from the example data, and $E_{mv}$ is simulated noise.

We construct $N(v)$ as described before. We use the posterior mean estimate of `SpDiST` to compare with the estimates of alternatives. We compute posterior mean of $\boldsymbol{A}_v$ based on 2000 MCMC samples, after discarding 3000 samples as burn-in. For comparison, the competing methods are the `DiST` (Wong et al., 2016), and a non-spatial method, i.e., the least squares (LS) method (Niethammer et al., 2006). The LS method (Niethammer et al., 2006) is to estimate $\boldsymbol{A}_v$ via

$$\arg\min_{\boldsymbol{A}_v} \sum_m \left|\left| \log S_{mv} - \log S_{0v} - b\boldsymbol{g}_m^T \boldsymbol{A}_v \boldsymbol{g}_m \right|\right|^2.$$

For `DiST`, the estimates are the principal eigenvectors. For comparison, we compute the principal eigenvectors of the posterior means of the diffusion tensor (for `DiST`), and the classical diffusion tensor estimate (for LS).

To quantify the performance of the three methods, we introduce two metrics. For voxels with fiber directions, we use *Metric 1*, defined as

$$d_1(\boldsymbol{m}_v, \hat{\boldsymbol{m}}_v) = \arccos\big(|\boldsymbol{m}_v^T \hat{\boldsymbol{m}}_v|\big),$$

, measuring the acute angle between true tensor direction $\boldsymbol{m}_v$ and estimated $\hat{\boldsymbol{m}}_v$. A small $d_1(\boldsymbol{m}_v, \hat{\boldsymbol{m}}_v)$ indicates that the fiber direction is estimated accurately. We also introduce *Metric 2*, measuring the difference between true between-neighbor angle and estimated between-neighbor angle, defined as:

$$d_2(\hat{\boldsymbol{m}}_v, \hat{\boldsymbol{m}}_u) = \Big|\arccos\big(|\hat{\boldsymbol{m}}_v^T \hat{\boldsymbol{m}}_u|\big) - \arccos\big(|\boldsymbol{m}_v^T \boldsymbol{m}_u|\big)\Big|,$$

where $u, v$ are neighbors. A small $d_2(\boldsymbol{m}_v, \hat{\boldsymbol{m}}_u)$ corresponds to an accurate decision, if the two voxels belong to the same fiber.

We summarize the results in Table 1, including the mean estimates by averaging over 200 replications. We observe that SpDiST and DiST have an overall better performance in comparison to the non-spatial method. From Table 1, SpDiST is more robust to noise, which may motivate a study on the robustness of tensor direction estimates based on different parameterization. However, the noise may have little effect on *Metric 2*, leading to the same fiber tracking results. Although SpDiST and DiST have similar performances, the MCMC-based SpDiST provides a way to quantify the uncertainties of fiber tracking, unlike DiST.

Table 1: Summary of simulation results based on *Metric 1* and *Metric 2*. Table entries are the averaged values of a certain metric, obtained by averaging over replications and voxels, from the fits of the LS, SpDiST and DiST methods.

| Metric | Noise ($\tau$) | Least squares | SpDiST | DiST |
|---|---|---|---|---|
| $d_1$ | 0.1 | 0.09 | 0.08 | 0.08 |
| | 0.5 | 0.19 | 0.12 | 0.17 |
| $d_2$ | 0.1 | 0.06 | 0.06 | 0.06 |
| | 0.5 | 0.23 | 0.08 | 0.09 |

# 5 Discussion

In this paper, we present a probabilistic dMRI fiber tracking approach using the spatial DAGAR proposal for modeling p.d. tensors. Although our analysis reveals similar performances for the DiST and SpDiST methods, the SpDiST method powered by MCMC approaches provides an elegant probabilistic quantification of the fiber tracking results, which may provide potentially important information to neuroscientists for understanding the anatomical connections in the brain. Furthermore, we also present sensitivity analysis to the tuning parameter $C$, addressing the issue raised by Kang and Li (2016).

Like various other modeling approaches in neurostatistics, our proposal also has various limitations. A majority of the current methods focus on developing an image processing tool, but not on scientifically and statistically valid explanations of the outcomes (Lazar et al., 2016). In that vein, proposing an appealing (regression) framework that characterizes various factors affecting the outcomes might be critical to advancing the field, and providing more insightful information. However, this continues to be challenging, as incorporating covariate information into a fiber tracking algorithm is not straightforward. Another important issue that persists is crossing fibers, where, the popular single tensor model (Mori et al., 1999) fails to account for voxels where there are multiple fibers. Although it is assumed that increasing the resolution of the image may handle this issue, Schilling et al. (2017) present an unexpected result that increasing the resolution may not a solution. All these remain as important avenues for future research, which may only foster with close interdisciplinary collaborations. The codes are available at the GitHub repository is

`https://github.com/ZhouLanNCSU/Probalistic_Fiber_Tracking`,

## Acknowledgements

The authors would like to thank the anonymous associate editor and the reviewer, whose constructive comments led to an improved version of the manuscript. Research of Reich and Bandyopadhyay were partially supported by grants R01DE024984 from the United States National Institutes of Health

## References

Bammer, R., Holdsworth, S. J., Veldhuis, W. B., and Skare, S. T. (2009), "New methods in diffusion-weighted and diffusion tensor imaging," *Magnetic resonance imaging clinics of North America*, 17, 175–204.

Behrens, T. E., Berg, H. J., Jbabdi, S., Rushworth, M. F., and Woolrich, M. W. (2007), "Probabilistic diffusion tractography with multiple fibre orientations: What can we gain?" *Neuroimage*, 34, 144–155.

Cheng, P., Magnotta, V. A., Wu, D., Nopoulos, P., Moser, D. J., Paulsen, J., Jorge, R., and Andreasen, N. C. (2006), "Evaluation of the GTRACT diffusion tensor tractography algorithm: a validation and reliability study," *Neuroimage*, 31, 1075–1085.

Chung, H.-W., Chou, M.-C., and Chen, C.-Y. (2011), "Principles and limitations of computational algorithms in clinical diffusion tensor MR tractography," *American Journal of Neuroradiology*, 32, 3–13.

Datta, A., Banerjee, S., Hodges, J. S., Gao, L., et al. (2019), "Spatial disease mapping using Directed Acyclic Graph Auto-Regressive (DAGAR) models," *Bayesian Analysis*, 14, 1221–1244.

Descoteaux, M., Deriche, R., Knosche, T. R., and Anwander, A. (2008), "Deterministic and probabilistic tractography based on complex fibre orientation distributions," *IEEE transactions on Medical Imaging*, 28, 269–286.

Dryden, I. L., Koloydenko, A., and Zhou, D. (2009), "Non-Euclidean statistics for covariance matrices, with applications to diffusion tensor imaging," *The Annals of Applied Statistics*, 1102–1123.

Kang, J. and Li, L. (2016), "Discussion of "Fiber direction estimation in diffusion MRI"," *The Annals of Applied Statistics*, 10, 1162.

Lazar, N. A. et al. (2016), "Discussion of "Fiber direction estimation in diffusion MRI"," *The Annals of Applied Statistics*, 10, 1160–1161.

Mori, S. (2007), *Introduction to Diffusion Tensor Imaging*, Elsevier.

Mori, S., Crain, B. J., Chacko, V. P., and Van Zijl, P. C. (1999), "Three-dimensional tracking of axonal projections in the brain by magnetic resonance imaging," *Annals of Neurology: Official Journal of the American Neurological Association and the Child Neurology Society*, 45, 265–269.

Morris, D. M., Embleton, K. V., and Parker, G. J. (2008), "Probabilistic fibre tracking: differentiation of connections from chance events," *Neuroimage*, 42, 1329–1339.

Niethammer, M., Estepar, R. S. J., Bouix, S., Shenton, M., and Westin, C.-F. (2006), "On diffusion tensor estimation," in *2006 International Conference of the IEEE Engineering in Medicine and Biology Society*, IEEE, pp. 2622–2625.

Schilling, K., Gao, Y., Janve, V., Stepniewska, I., Landman, B. A., and Anderson, A. W. (2017), "Can increased spatial resolution solve the crossing fiber problem for diffusion MRI?" *NMR in Biomedicine*, 30, e3787.

Schlaier, J. R., Beer, A. L., Faltermeier, R., Fellner, C., Steib, K., Lange, M., Greenlee, M. W., Brawanski, A. T., and Anthofer, J. M. (2017), "Probabilistic vs. deterministic fiber tracking and the influence of different seed regions to delineate cerebellar-thalamic fibers in deep brain stimulation," *European Journal of Neuroscience*, 45, 1623–1633.

Soares, J. M., Marques, P., Alves, V., and Sousa, N. (2013), "A hitchhiker's guide to diffusion tensor imaging," *Frontiers in Neuroscience*, 7.

Sporns, O., Tononi, G., and Kötter, R. (2005), "The human connectome: A structural description of the human brain," *PLoS Computational Biology*, 1, e42.

Wong, R. K., Lee, T. C., Paul, D., Peng, J., ADNI, et al. (2016), "Fiber direction estimation, smoothing and tracking in diffusion MRI," *The Annals of Applied Statistics*, 10, 1137–1156.

*Received: March 16, 2021*

*Accepted: April 20, 2021*